Supporting Information

Triboelectric Effect of Surface Morphology controlled Laser Induced Graphene

Kwang-Hun Choi[a,b], Seoungwoong Park[a,c], Seok-Ki Hyeong[a], Sukang Bae[a], Jae-Min Hong[a], Tae-Wook Kim[d], Sang Hyun Lee[e], Seongwoo Ryu[b*] and Seoung-Ki Lee[a*]

a. Functional Composite Materials Research Center, Korea Institute of Science and Technology (KIST), 92 Chudong-ro, Bongdong-dup, Wanju-gun, Jeallabuk-do, 55324, Republic of Korea

b. Department of Polymer Engineering, College of Engineering, Suwon University, 17 Wauan-gil, Bongdam-eup, Hwaseong-si, Gyeonggi-do, 18323, Republic of Korea

c. Department of Chemistry, Seoul National University, 1 Gwanak-ro, Gwanak-gu Seoul 08826, Republic of Korea

d. Department of Flexible and Printable Electronics, Jeonbuk National University, Jeonju, Jeonbuk 54896, Korea

e. School of Chemical Engineering, Chonnam National University, 77 Yongbongro, Buk, Gwangju 61186, Republic of Korea

Figure S1. Cross section SEM images of (a) LIG, (b) SF-LIG and (c) LF-LIG in order of left to right. Inset image of figure (a) exhibited porous cross section of structure of LIG (scale bar = 5 μm). The area converted to LIG is indicated by a yellow dashed line.

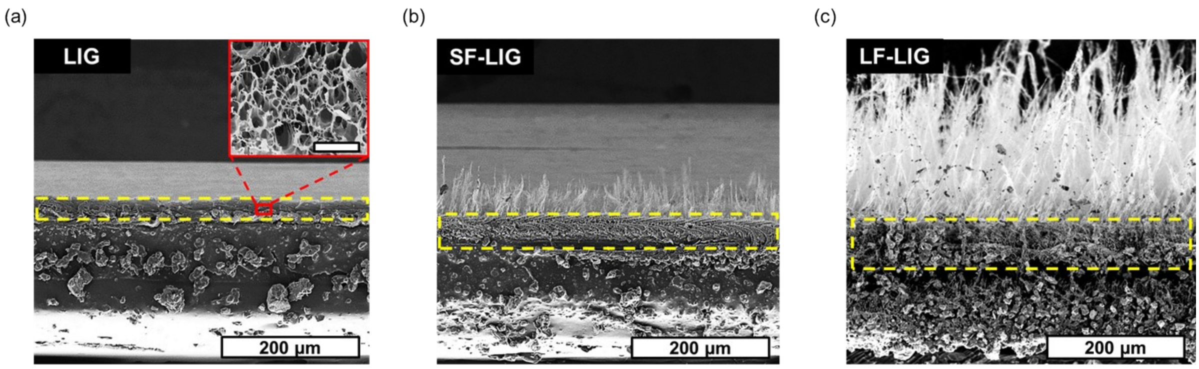

Figure S2. Optical photographs of laser scribed region of PI under respective working distances (from -0.9 to 1.2 mm). At working distance -0.9 mm, width of formed LIG was ~ 160 μm and it became narrower to 60 μm at a focal point. As expected, the spot size becomes larger again (diameter of spot = 150 μm) when refocusing the substrate to +1.2 mm.

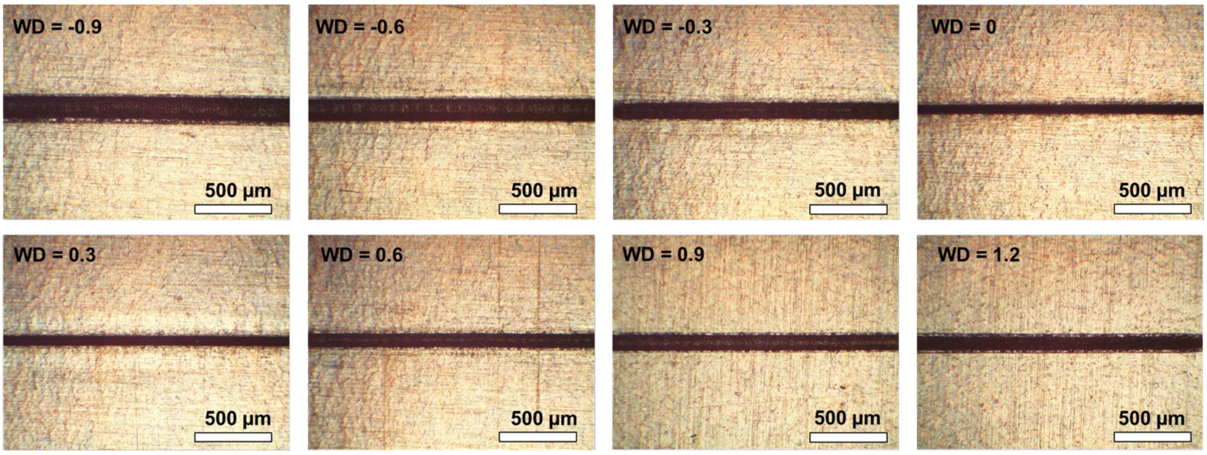

Figure S3. Deconvolution of the D and G bands of representative three types of LIGs. (a) LIG, (b) SF-LIG and (c) LF-LIG.

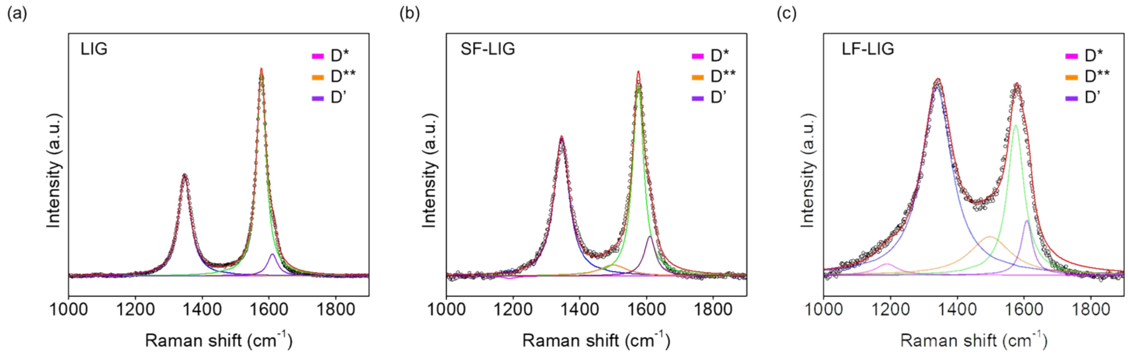

Figure S4. Schematic illustration of laser scribing of PI substrate at a different working distance and the effects on LIG synthesis.

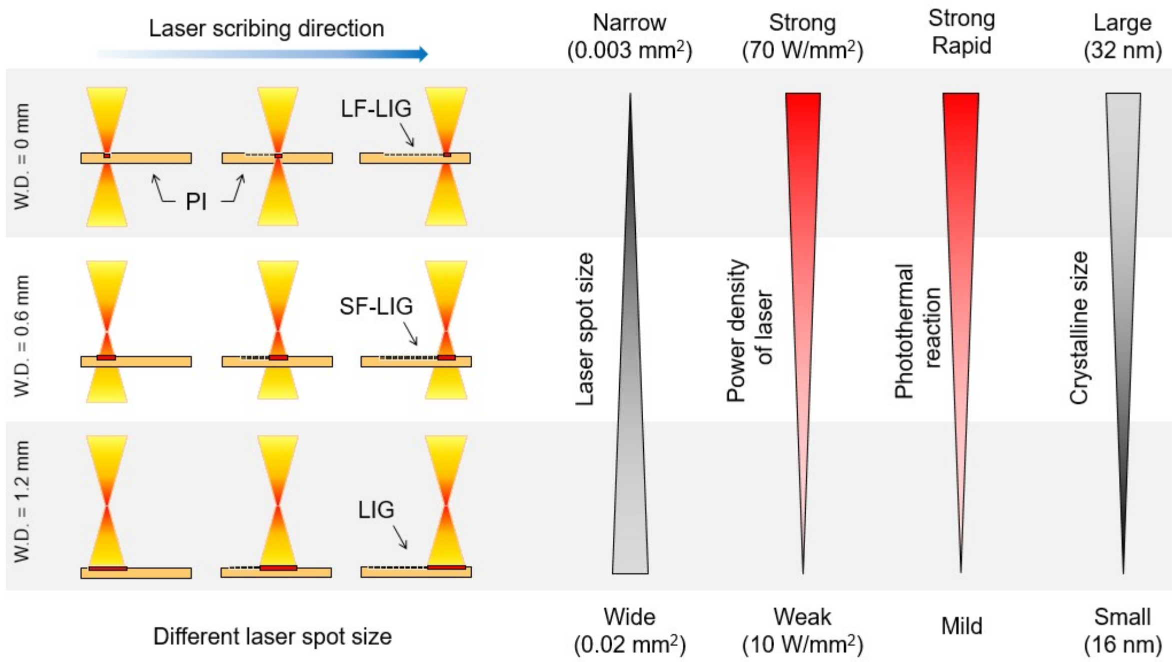

When the PI substrate is far from the focal plane (W.D. =1.2 mm), the laser with mild power density (~10 W/mm^2) is irradiated to the wide spot area of PI substrate, which sequentially induces depolymerization of PI, carbonization and graphitization. The synthesized LIG under this condition is a commonly known porous LIG, which is the optimum condition that can minimize the defects of LIG. On the other hand, when the PI substrate is placed in the focal plane (W.D. = 0 mm), the laser with high power density (~70 W/mm^2) is irradiated to the narrow spot area, inducing more rapid photothermal reaction. It is considered that the high energy density of laser causes overheating, thus lead an additional break of crystal structure such as stacking faults and lattice symmetry breaking, reducing the crystalline size.

Figure S5. Deconvoluted XPS core level spectra of (a) C 1s, (b) O 1s and (c) N 1s for polyimide film.

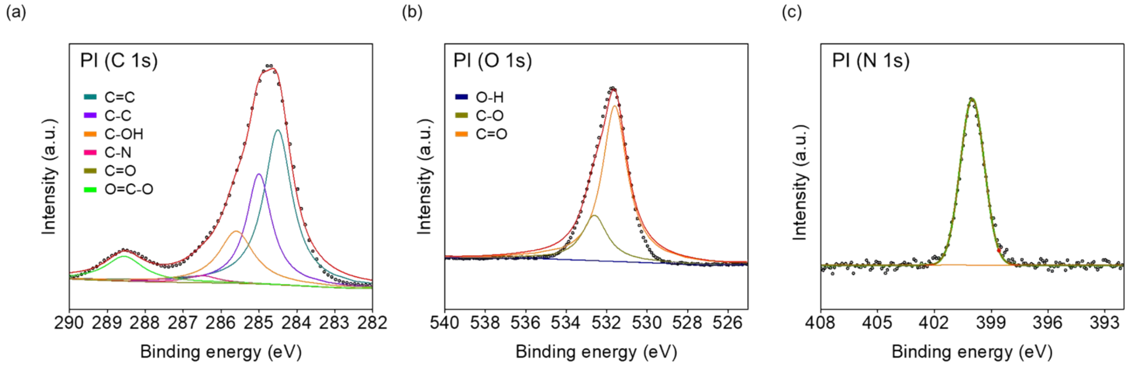

Figure S6. Deconvoluted XPS core level spectra of (a-c) C 1s and (d-f) O 1s for three types of LIGs.

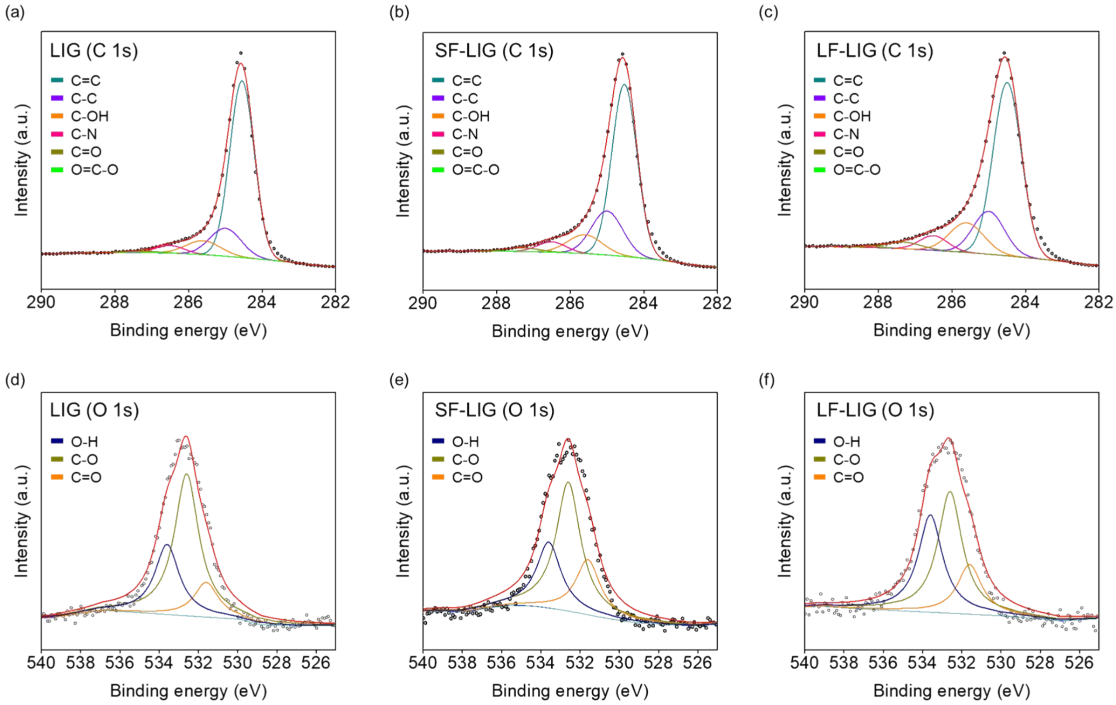

Figure S7. Schematic illustration of LF-LIG based TENG operation mechanism, charge flows upon press/release behavior is induced from contact electrification effect between triboelectric layer.

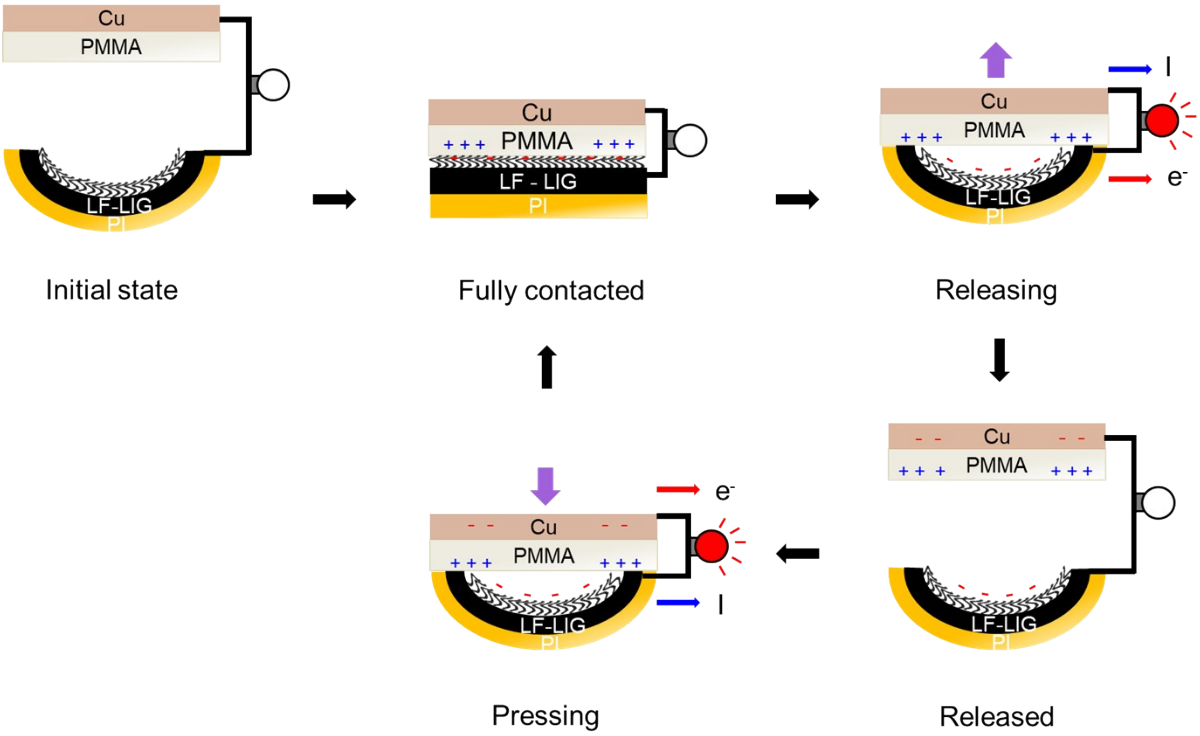

Physically isolated two triboelectric active layers (LF-LIG/PMMA) has no induced charge. When they are brought in to contact with each other, each layers surfaces are spontaneously charged in positive and negative states by contact electrification effect. Followed with above triboelectric series and surface charge potential, LF-LIG is negatively charged while PMMA is positively charged that chemical potential difference is induced between them. During the releasing process, this potential difference generated the charges flow from copper electrode of PMMA triboelectric active layers to LF-LIG for realize the energy balance. As these triboelectric active layers brought back in to contact with pressing process, charges flow back in the reverse direction through the external load.

Figure S8. (a) Schematic illustration and (b) electrical output performance of fabricated LIG and LF-LIG based TENG with 'Acrylic' counter material. (c) schematic illustration and (d) electrical output performance of fabricated LIG and LF-LIG based TENG with 'PET' as a counter material.

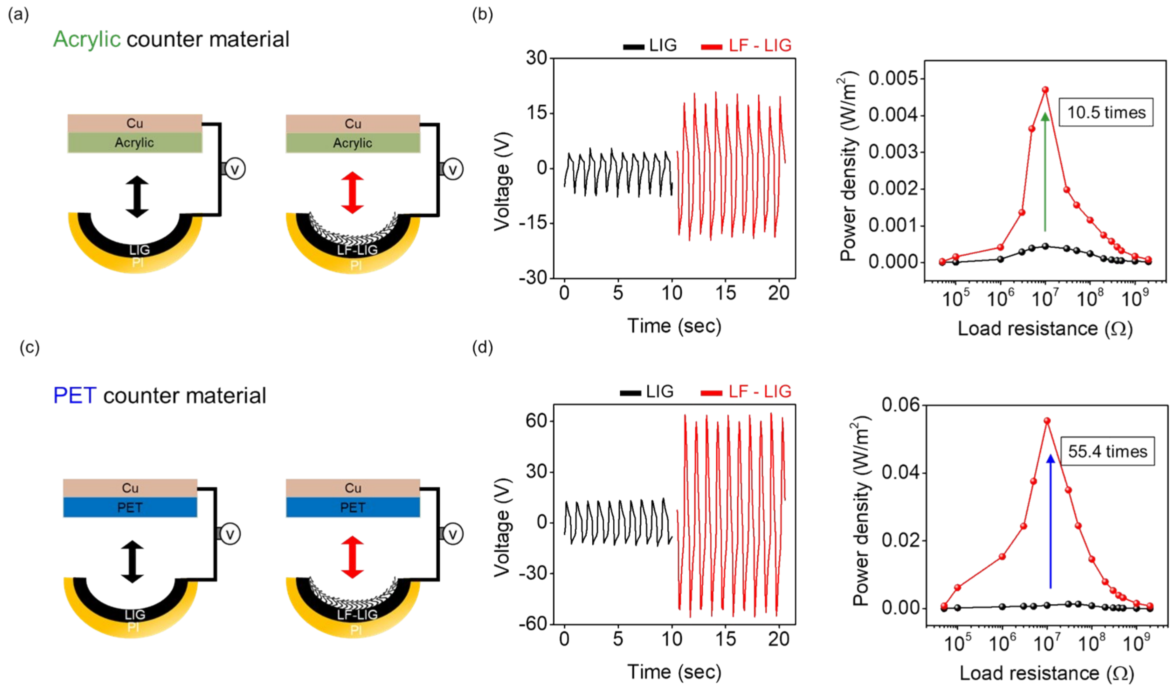

Figure S9. (a) Schematic of circuit diagram for powering electronic devices. (b) Photograph of fabricated TENG circuit, connected serially with rectifying diode and 100 ea LEDs.

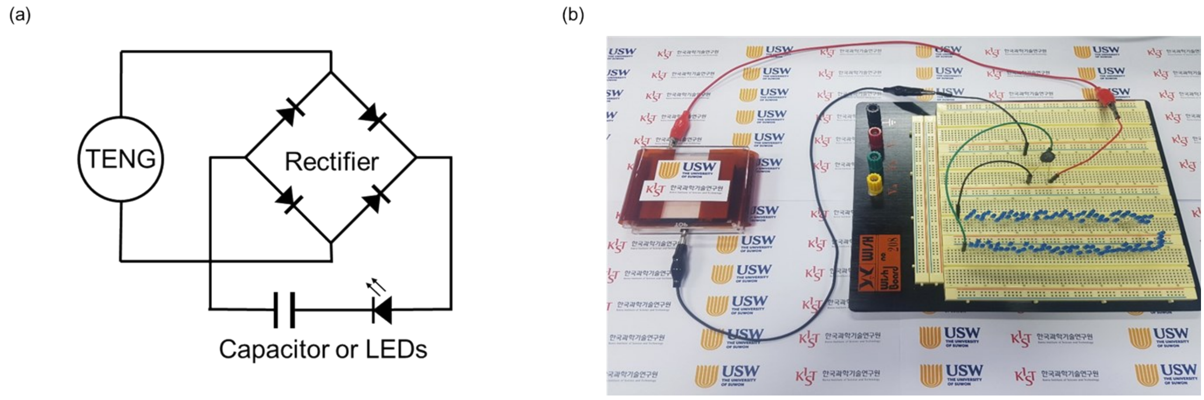

Figure S10. Photograph of single (a), double (b) and multi (c) touching behavior on matrixes of TENG touch sensor.

(a) (b) (c)

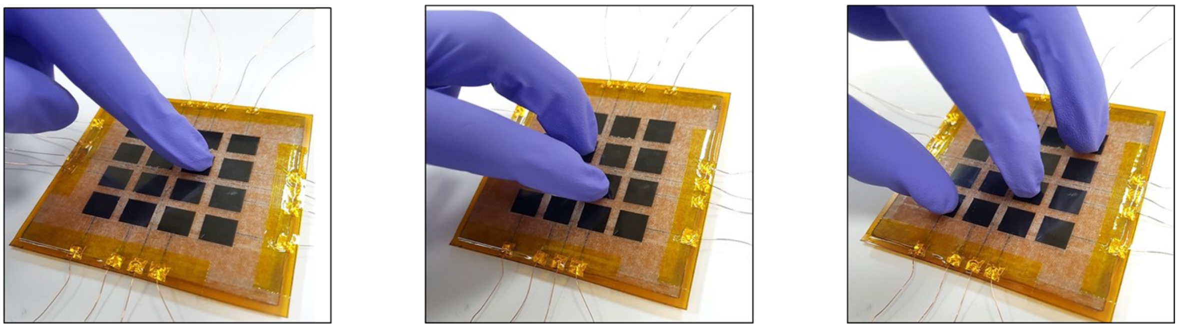

Figure S11. Real time output signals on respective pixels of 4 x 4 matrices under continuous dragging behavior, dragging direction is indicated with a red color arrow.

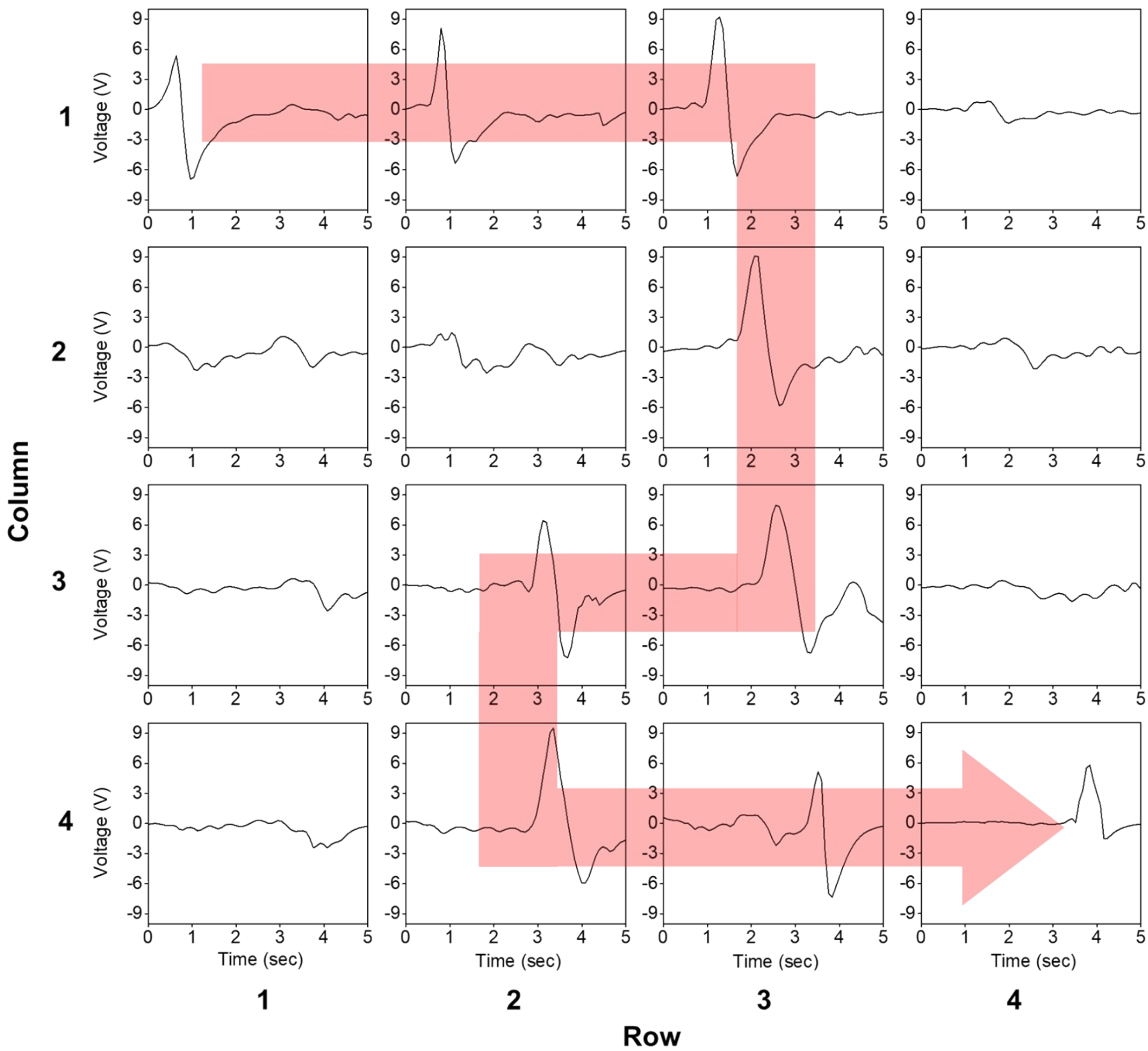

Table S1. Average and standard deviation of the height and sheet resistance of each LIGs, which is the data from 10 samples synthesized in separate batches.

Sample #	Height (μm)			Sheet resistance (Ω/sq)		
-	LIG	SF-LIG	LF-LIG	LIG	SF-LIG	LF-LIG
1	7	98	292	33.48	52.49	76.15
2	6	114	283	42.08	52.77	77.79
3	5	111	264	27.43	50.39	78.69
4	6	90	264	28.90	50.97	77.99
5	7	91	256	26.65	48.72	81.44
6	5	96	298	24.84	48.42	76.05
7	8	96	278	34.24	48.38	82.82
8	5	98	259	32.56	49.88	77.33
9	6	102	288	23.49	51.50	81.29
10	5	104	294	42.06	52.81	79.11
Average	6	100	277.6	31.57	50.63	78.87
Standard deviation	±1.1	±7.87	±15.68	±6.59	±1.76	±2.30